Research article

IRF8 maintains mononuclear phagocyte and neutrophil function in acute kidney injury☆

Na Li [a,b,1], Stefanie Steiger [c,1], Ming Zhong [a,1], Meihua Lu [d,1], Yan Lei [a], Chun Tang [a], Jiasi Chen [a], Yao Guo [b], Jinhong Li [a], Dengyang Zhang [b], Jingyi Li [e], Enyi Zhu [a], Zhihua Zheng [a,****,2], Julia Lichtnekert [c,***,2], Yun Chen [b,2,**], Xiaohua Wang [a,2,*]

[a] Department of Nephrology, Center of Kidney and Urology, The Seventh Affiliated Hospital, Sun Yat-Sen University, 518107, Shenzhen, China
[b] Scientific Research Center, Edmond H. Fischer Translational Medical Research Laboratory, The Seventh Affiliated Hospital, Sun Yat-Sen University, 518107, Shenzhen, China
[c] Renal Division, Department of Medicine IV, Ludwig-Maximilians-University Hospital, Ludwig-Maximilian-University Munich, 80336, Munich, Bavaria, Germany
[d] Department of Geriatrics, People's Hospital of Banan District, 401320, Chongqing, China
[e] Department of Pulmonary & Critical Care Medicine, Shenzhen Hospital of Southern Medical University, 518107, Shenzhen, China

ARTICLE INFO

ABSTRACT

Immune cells are key players in acute tissue injury and inflammation, including acute kidney injury (AKI). Their development, differentiation, activation status, and functions are mediated by a variety of transcription factors, such as interferon regulatory factor 8 (IRF8) and IRF4. We speculated that IRF8 has a pathophysiologic impact on renal immune cells in AKI and found that IRF8 is highly expressed in blood type 1 conventional dendritic cells (cDC1s), monocytes, monocyte-derived dendritic cells (moDCs) and kidney biopsies from patients with AKI. In a mouse model of ischemia–reperfusion injury (IRI)-induced AKI, $Irf8^{-/-}$ mice displayed increased tubular cell necrosis and worsened kidney dysfunction associated with the recruitment of a substantial

amount of monocytes and neutrophils but defective renal infiltration of cDC1s and moDCs. Mechanistically, global *Irf8* deficiency impaired moDC and cDC1 maturation and activation, as well as cDC1 proliferation, antigen uptake, and trafficking to lymphoid organs for T-cell priming in ischemic AKI. Moreover, compared with $Irf8^{+/+}$ mice, $Irf8^{-/-}$ mice exhibited increased neutrophil recruitment and neutrophil extracellular trap (NET) formation following AKI. IRF8 primarily regulates cDC1 and indirectly neutrophil functions, and thereby protects mice from kidney injury and inflammation following IRI. Our results demonstrate that IRF8 plays a predominant immunoregulatory role in cDC1 function and therefore represents a potential therapeutic target in AKI.

1. Introduction

Ischemia–reperfusion injury (IRI) is a common cause of acute kidney injury (AKI) and can eventually lead to chronic kidney disease (CKD) and even progress to end-stage kidney disease [1]. IRI is associated with tissue injury (tubular cell necrosis with release of pathogen- or danger-associated molecular patterns (PAMPs or DAMPs)) and extensive intrarenal inflammation (infiltration and activation of leukocytes, including neutrophils and mononuclear phagocytes (MPCs, such as monocytes, dendritic cells and macrophages)) and release of proinflammatory mediators; processes referred to as necroinflammation [2,3].

Dendritic cells (DCs) are sentinels during IRI-induced AKI. DCs primarily produce tumor necrosis factor-α (TNF-α) and drive naive T-cell differentiation to attract more neutrophils and other immune effector cells [4], therefore promoting tissue injury and inflammation. DCs can also upregulate the expression of costimulatory molecules and CCR7 and migrate to secondary lymphoid tissues for processing and antigen presentation to T cells, leading to T lymphocyte proliferation [5]. Moreover, recent evidence suggests that a subset of DCs, specifically the type 1 conventional dendritic cell (cDC1) subset, promotes the expression of anti-inflammatory reparative cytokines such as IL-10 and IL-22 and antagonizes the proinflammatory Th1 immune response and the recruitment of neutrophils; thus, cDC1s can diminish kidney injury [6,7].

Mechanistically, PAMPs or DAMPs are recognized via Toll-like receptors (TLRs) [8] as well as cytoplasmic dsRNA sensors such as retinoic acid-inducible gene I (RIG-I) and melanoma differentiation antigen 5 (MDA5), which signal through the adaptor molecule mitochondrial antiviral signaling protein (MAVS) [9], in DCs, monocytes and macrophages. Both, the TLR and RIG-I/MDA5 signaling pathway intersect at the level of interferon regulatory factors (IRFs) [10]. IRFs are a group of transcription factors that function as interferon consensus sequence-binding proteins. IRF8 can regulate transcription through multiple target DNA elements and functions as either activator or repressor depending on the formation of different heterodimeric complexes [11–14]. Evidence suggests that IRF8-PU.1 heterodimer binds to the ETS-IRF composite element or IRF-ETS composite sequence to drive H3K3me1 monomethylation in monocytes [15], while the IRF8-Baft3 heterodimer activates the protein-1-IRF composite element to promote gene activation related to cDC1 differentiation [13,14,16]. In macrophages and DC precursors (MDPs) and common monocyte progenitors (cMoPs), IRF8 directly interacts with CCAAT enhancer-binding protein-α (C/EBPα) and inhibits chromatin binding and transactivation activities of C/EBPα, thereby blocking neutrophil differentiation [11,12,17]. Moreover, the inactivation of krüppel-like factor-4 (KLF4) caused by *Irf8* loss increases neutrophil adhesion and neutrophil extracellular trap (NET) formation [18,19]. IRF8 also regulates the adaptive immune response, type I IFN production [16,20,21] and antigen presentation [22].

Despite such findings on the role of IRF8 in disease, the underlying mechanisms in AKI are not fully elucidated: 1) How does IRF8 control cDC1s to protect the kidney from IRI-induced AKI [6]; and 2) Does IRF8 regulate monocyte and neutrophil functions in AKI [23,24]. Thus, we hypothesized that IRF8 modulates leukocyte recruitment, differentiation, and function during the early stages of IRI-induced AKI.

2. Materials and methods

2.1. Design of the human study

This study included three distinct patient cohorts. 1) The first cohort comprised 15 patients with AKI (diagnosed with hypovolemia-induced AKI after admission). Blood specimens were collected on the 1st, 2nd, and 3rd day after admission. 19 healthy individuals without kidney impairment were included as a control group (healthy group). Patients with a history of CKD or immunosuppressive drug treatment prior to/during admission were excluded. 2) The second cohort included 4 biopsies from 4 different kidney transplant donors. All kidneys underwent wedge biopsy before transplantation and the donors were considered healthy individuals. A second graft biopsy was performed 7–15 days after transplantation, which included Patient 1 (8 days after transplantation), Patient 2 (10 days after transplantation), and Patient 3 (14 days after transplantation). Each kidney biopsy specimen was immediately embedded in paraffin. 3) The third cohort consisted of 12 patients pathologically diagnosed with acute tubular injury, none of whom exhibited a history of CKD or immunosuppressive drug treatment prior to/during admission. The entire study was approved by the Ethics Committee of the Seventh Affiliated Hospital of Sun Yat-Sen University (KY-2022-025-02, KY-2023-081-01).

2.2. Isolation of human blood mononuclear cells (PBMCs)

Whole blood samples (2 ml) were isolated from the first cohort on the 1st, 2nd, and 3rd day after admission. PBMCs were purified as indicated [25]. Finally, the cells were used for flow cytometric analysis.

2.3. Animal studies

$Irf8^{-/-}$ (C57BL/6J-$Irf8^{em1Cya}$) mice bearing a deletion of exons 3–6 in the transcriptional start site of IRF8 were generated at Cyagen using a previously reported strategy [26]. The decrease in IRF8 RNA expression in healthy kidneys was confirmed by RNA sequencing (unpublished data). The mice were bred at the laboratory animal center of Sun Yat-Sen University (Guangzhou, China). Groups of five mice were housed under specific pathogen-free (SPF) conditions with unlimited access to food and water and a 12-h light cycle. Eight-week-old male mice were used for further experiments. The following mouse lines were used: wild-type C57BL/6 mice, $Irf8^{-/-}$ mice and littermate $Irf8^{+/+}$ mice.

2.4. Mouse model of IRI-induced AKI

IRI surgery was performed as previously described [27]. Mice were anesthetized to achieve analgesia, amnesia, and hypnosis. Online rectal temperature data were recorded for every mouse after anesthesia. Body temperature was monitored and remained stably around 37 °C. The duration of ischemia applied was 25 min after unilateral renal pedicle clamping. Successful perfusion was assessed by a change in color from pale to the original color. Afterward, wounds were closed and 500 μl of saline applied to balance fluid loss. After 1 day or 7 days, blood collection was performed, and the mice were sacrificed by cervical dislocation. Kidneys were transferred to 4 % paraformaldehyde (PFA) for histology, frozen for qRT–PCR analysis or kept on ice for flow cytometry analysis.

2.5. Isolation of kidney MPCs and flow cytometry

Kidneys were isolated, harvested and processed as described in a previous study [6]. AccuCheck counting beads (Thermo Fisher Scientific, USA) were used, and the absolute number of renal cell subsets per microliter was calculated according to the manufacturer's instructions.

All the following anti-mouse Abs were obtained from BioLegend (USA): CD16/32 Fcblock, AF488-CCR7, AF700-CD45, APC-CD40, APC-CD64, APC/Cy7-CD11c, BV421-CD8, BV421-XCR1, BV510-CD4, BV510-MHC II, BV605-D49, BV605-CD64, BV650-Ly6g, BV785-CD19, BV785-CD86, FITC-Ly6c, PE-CD123, PE/Cy5-CD80, PE/Cy7-CD11b, and PerCP/Cy5.5-CD3e. The following anti-human Abs were obtained from BioLegend (USA): APC/Cy7-CD11c, BV510-CD1c, BV650-HLA-DR, FITC-CD15, PerCP/Cy5.5-CD3, PE-CD19, Pacific Blue-CD123, PE/Cy7-CD141, and human TruStain FcX™. Additionally, V500-conjugated anti-human CD14 was purchased from BD Biosciences (USA), and APC-conjugated anti-mouse/human IRF8 was purchased from eBioscience (USA).

2.6. Histology

Human and mouse kidneys were embedded in paraffin. Two-micron-thick kidney sections were prepared for periodic acid-Schiff (PAS) staining. Representative images of kidneys are shown. Injured tubular index was scored by the percentage of tubules in the corticomedullary junction that displayed cell necrosis, loss of brush border, cast formation, edema, and tubular dilation as follows: 0, none; 1, ≤10 %; 2, 11–25 %; 3, 26–45 %; 4, 46–75 %; 5, >76 % [6].

For immunohistochemical or immunofluorescence staining, the following primary anti-human Abs were used: rabbit anti-IRF8 (1:500, Abcam, USA) and mouse anti-HLA-DR (1:500, Abcam, USA). The following anti-mouse Abs were used: rabbit IRF8 (1:500, Abcam, USA), rabbit Ly6g (1:500, Servicebio, China), rabbit myeloperoxidase (MPO, 1:500, Servicebio, China), rabbit THP-1 (1:100, Servicebio, China), rabbit aquaporin-1 (AQP1, 1:200, Servicebio, China), rabbit CCR2 (1:100, Servicebio, China), and rabbit CD11b (1:200, Servicebio, China). All assessments were performed by two blinded observers (N.L. and M.Z.).

2.7. Immunofluorescence microscopy

As previously described [25], paraffin-embedded mouse kidney sections were incubated in dewaxing and clearing solutions and dehydrated in pure ethanol. The tissue was covered with 3 % BSA for 30 min at RT. Subsequently, the slides were incubated with primary Abs. After washing, the membranes were incubated with the corresponding secondary Abs for 40 min at RT. Finally, the sections were counterstained with DAPI for 10 min in the dark, mounted, and stored at 4 °C until imaging. Fluorescence scanning was performed with a Panoramic Midi II (3DHistech, Hungary) instrument equipped with multiple lasers. The following channel settings were used: DAPI (excitation, 365 nm; emission, 420–470 nm; blue), FITC (484–504 nm; 517–537 nm; green), and CY3 (576–596 nm; 618–638 nm; red). Slide images were acquired at 43x and 86× magnification, and the image voxel size was 0.087 μm/pixel. All scanned slides were imported into Caseviewer 2.3 to adjust the brightness/contrast, add scale bars, and obtain pictures.

2.8. Blood urea nitrogen (BUN) and creatinine (CR) levels

As indicated, reagents R1 (Composed of creatinease, peroxidase, sarcosine oxidase, ascorbic acid oxidase, and TOPS) and R2

(Composed of creatinase, 4-AAP) were mixed according to the manufacturer's instructions (Rayto, China). The corresponding parameters were set on an automatic biochemical analyzer (Chemray 800; Rayto, China), and then the serum samples were loaded. The results were exported after the automatic biochemical analyzer was run, and the results were acquired in Excel format.

2.9. Quantitative real-time PCR (qRT−PCR)

A Pure Link RNA Mimi Kit (Invitrogen™, USA) was used to extract total RNA from mouse kidneys stored in RNAlater and mouse MPCs stored in lysis buffer according to the manufacturer's instructions. cDNA was synthesized from 2 µg of total RNA by reverse transcription polymerase chain reaction (PCR) using 5x *Evo M-MLV* RT Master Mix consisting of RTase, an RNase inhibitor, dNTPs, oligo dT (18T) primers, random 6-mer primers, and reaction buffer (Accurate Biotechnology, China). Reverse transcription was performed at 37 °C for 15 min and 85 °C for 5 s using a Mastercycler Pro.

Quantitative real-time PCR of cDNA was performed using a SYBR® Green Premix Pro Taq HS qPCR Kit (Accurate Biotechnology, China). The reactions were performed using a Light Cycler 480 (Roche, Germany) with a SYBR green PCR detection system. Negative controls containing ddH2O were use to assess the target and reference genes. Each amplification step included an initiation phase at 95 °C, an annealing phase at 60 °C and an amplification phase at 72 °C, and each step was repeated for 40 cycles. Primers were designed to be cDNA specific and target most CCDS-approved transcripts. All samples that did not exceed the background fluorescence (crossing point/quantification cycle) of 35 cycles during the amplification reaction were considered not detectable. The melting curve profiles were analyzed for every sample to identify unspecific products and primer dimers. The products were visualized on agarose gels. All gene expression values were normalized to that of 18S rRNA, which was used as a housekeeping gene, and calculated using the following equation: $2^{-\Delta [CT_{gene}-CT_{18s\ rRNA}]}$. All murine primers used for amplification were purchased from Origene and are listed in Table 1.

2.10. ELISA

The levels of MPO (FINETEST, Wuhan, China), citrullinated histone 3 (Cit-H3, Meimian, Jiangsu, China), and neutrophil elastase (NE, FINETEST, Wuhan, China) were measured at a 1:5 dilution according to the manufacturer's instructions.

2.11. EdU in vivo injection

For *in vivo* labeling, 10 mg/ml EdU was prepared in sterile D-PBS. EdU (0.1 mg/g body weight) was injected i.p. After 12 h, the kidneys were harvested and digested. EdU was detected by using a Click-iT EdU Alexa Fluor 647 flow cytometry assay kit (Thermo Fisher Scientific, USA).

Table 1
Murine primer sequences.

| Mouse Genes	Primer Sequences
Ccl2	Forward 5′-GCTACAAGAGGATCACCAGCAG-3′; Reverse 5′-GTCTGGACCCATTCCTTCTTGG-3′
Ccl3	Forward 5′-ACTGCCTGCTGCTTCTCCTACA-3; ′ Reverse 5′-ATGACACCTGGCTGGGAGCAAA-3′
Ccl17	Forward 5′-CGAGAGTGCTGCCTGGATTACT-3′; Reverse 5′-GGTCTGCACAGATGAGCTTGCC-3′
Ccl19	Forward 5′-TCGTGAAAGCCTTCCGCTACCT-3′; Reverse 5′-CAGTCTTCGGATGATGCGATCC-3′
Ccl21a	Forward 5′-GGGTCAGGACTGCTGCCTTAAG-3′; Reverse 5′-AGCTCAGGCTTAGAGTGCTTCC-3′
Ccl21b	Forward 5′-TCCCTACAGTATTGTCCGAGGC-3′; Reverse 5′-ATCAGGTTCTGCACCCAGCCTT-3′
Ccr1	Forward 5′-GCCAAAAGACTGCTGTAAGAGCC-3′; Reverse 5′-GCTTTGAAGCCTCCTATGCTGC-3′
Ccr2	Forward 5′-GCTGTGTTTGCCTCTCTACCAG-3′; Reverse 5′-CAAGTAGAGGCAGGATCAGGCT-3′
Ccr3	Forward 5′-CCACTGTACTCCCTGGTGTTCA-3′; Reverse 5′-GGACAGTGAAGAGAAAGAGCAGG-3′
Ccr4	Forward 5′-GGACTAGGTCTGTGCAAGATCG-3′; Reverse 5′-TGCCTTCAAGGAGAATACCGCG-3′
Ccr5	Forward 5′-GTCTACTTTCTCTTCTGGACTCC-3′; Reverse 5′-CCAAGAGTCTCTGTTGCCTGCA-3′
Ccr6	Forward 5′-ACAGAGCCATCCGAGTCGTGAT-3′; Reverse 5′-CTGGTGTAGGCGAGGACTTTCT-3′
Ccr7	Forward 5′-AGAGGCTCAAGACCATGACGGA-3′; Reverse 5′-TCCAGGACTTGGCTTCGCTGTA-3′
Ccr8	Forward 5′-CTGCGATGTGTAAGGTGGTCTC-3′; Reverse 5′-CCTCACCTTGATGGCATAGACAG-3′
Ccr9	Forward 5′-GCCATGTTCATCTCCAACTGCAC-3′; Reverse 5′-CCTTCGGAATCTCTCGCCAACA-3′
Ccr10	Forward 5′-CAGTCTTCGTGTGGCTGTTGTC-3′; Reverse 5′-TCACAGTCTGCGTGAGGCTTTC-3′
Cxcl12	Forward 5′-GGAGGATAGATGTGCTCTGGAAC-3′; Reverse 5′-AGTGAGGATGGAGACCGTGGTG-3′
Cxcl14	Forward 5′-TACCCACACTGCGAGGAGAAGA-3′; Reverse 5′-CGCTTCTCGTTCCAGGCATTGT-3′
Cx3cr1	Forward 5′-GAGCATCACTGACATCTACCTCC-3′; Reverse 5′-AGAAGGCAGTCGTGAGCTTGCA-3′
Cxcr4	Forward 5′-GACTGGCATAGTCGGCAATGGA-3′; Reverse 5′-GACTGGCATAGTCGGCAATGGA-3′
Ifn-α7	Forward 5′-TCCTGCCTGAAGGACAGAAAGG-3′; Reverse 5′-GGTCAGCTCATGCAGAACACAG-3′
Ifn-γ	Forward 5′-CAGCAACAGCAAGGCGAAAAAGG-3′; Reverse 5′-TTTCCGCTTCCTGAGGCTGGAT-3′
Ifn-κ	Forward 5′-ACTGGGAACGTATCAGATCGGG-3′; Reverse 5′-CAACTCCAGGTAGACTGTCAGG-3′
Il-18	Forward 5′-GACAGCCTGTGTTCGAGGATATG-3′; Reverse 5′-TGTTCTTACAGGAGAGGGTAGAC-3′
Kim1	Forward 5′-CTGGAATGGCACTGTGACATCC-3′; Reverse 5′-GCAGATGCCAACATAGAAGCCC-3′
Ngal	Forward 5′-ATGTCACCTCCATCCTGGTCAG-3′; Reverse 5′-GCCACTTGCACATTGTAGCTCTG-3′
Tim2	Forward 5′-CTCTACTTCTCCAACACCAGCAC-3′; Reverse 5′-CCAAGGGTCATCTGAGGATGTC-3′
18s	Forward 5′-GCAATTATTCCCCATGAACG-3′; Reverse 5′-AGGGCCTCACTAAACCATCC-3′
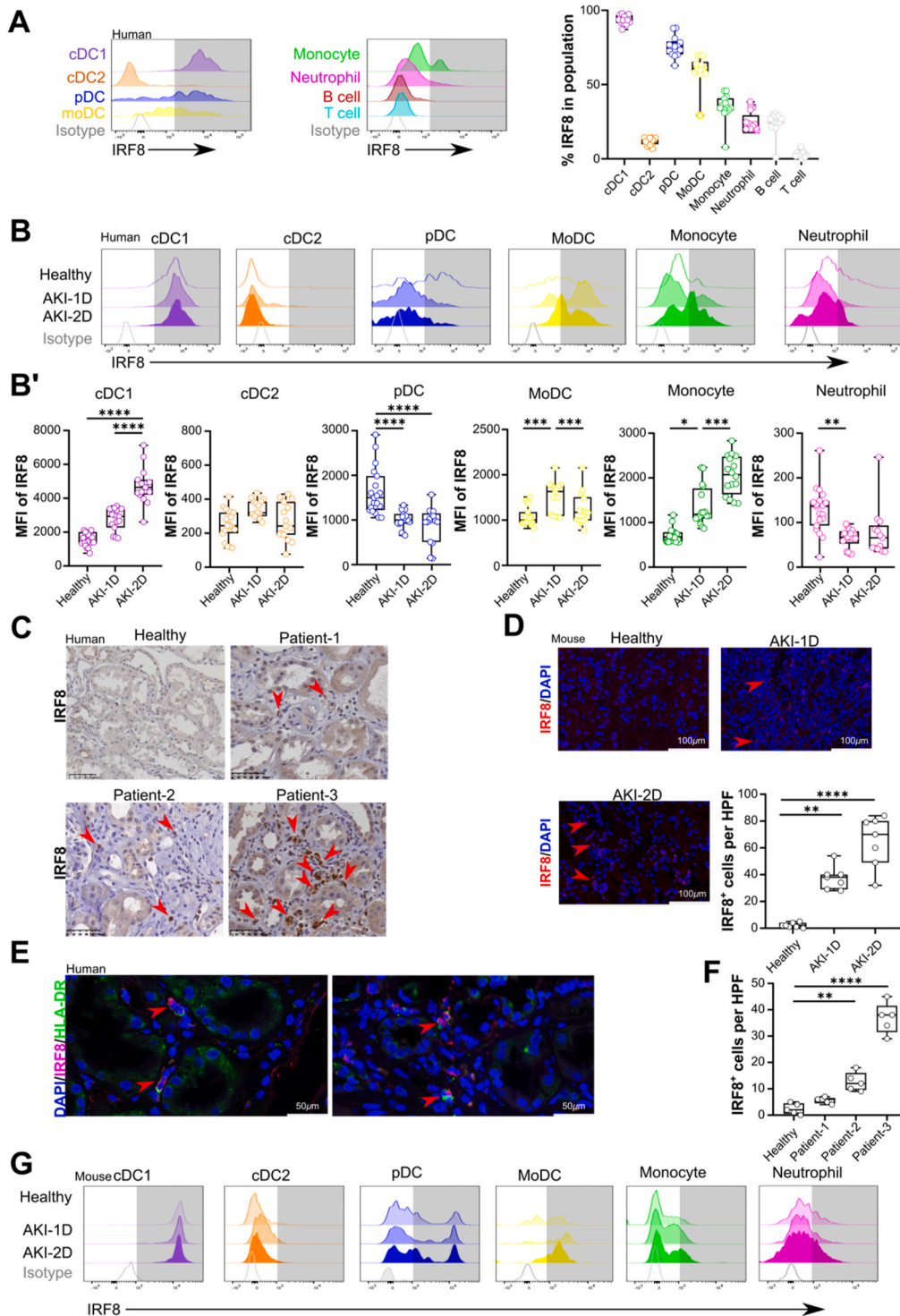
Fig. 1. Interferon regulatory factor 8 expression increases in patients and mice with acute kidney injury. (A) Histograms of IRF8 expression in human blood leukocytes from healthy individuals compared with isotype control staining ($n = 14$ per group). The gating strategy for blood leukocytes is shown in Supplemental Fig. 1. (B) The dynamic expression patterns of IRF8 in blood leukocytes from healthy individuals ($n = 14$ per group) and patients with AKI ($n = 10$ per group). (B′) MFI of IRF8 in the blood leukocyte populations in healthy individuals and patients with AKI. (C) Distribution and (F) number of IRF8-positive cells ($n = 1$ per group) in kidneys from transplantation patients. Red arrows indicate IRF8+ cells. Scale bar, 50 μm. (D) Mouse kidney sections were stained with anti-IRF8 (red) and DAPI (blue), and the numbers of IRF8+ cells are shown ($n = 6$ per group). Scale bar, 100 μm. Red arrow: IRF8+ cell. (E) Two representative images of co-staining for IRF8 and HLA-DR in kidney specimens from 12 patients pathologically diagnosed with acute tubular injury (n = 12 per group). Red arrow: IRF8+HLA-DR+ cell. Scale bar, 50 μm. (G) Dynamic

expression patterns of IRF8 in kidney leukocytes (gated as indicated inSupplemental Fig. 2A) from healthy mice and mice with AKI. The data are shown as the mean ± SD. *p < 0.05, **p < 0.01, ***p < 0.001, and ****p < 0.0001. One-way ANOVA. (For interpretation of the references to color in this figure legend, the reader is referred to the Web version of this article.)

2.12. Ovalbumin (OVA) uptake ex vivo

One day after AKI, MPCs were isolated from kidneys using a Percoll gradient under sterile conditions. A total of 1×10^5 cells were seeded in 200 μl of complete medium (RPMI 1640 medium supplemented with 10 % FBS, 1 % penicillin/streptomycin, L-glutamine, and 0.05 mM β-mercaptoethanol). The cells were cooled and incubated with 25 μg/ml OVA-AF488 (Invitrogen, USA) for 45 min on ice. After washing, the cells were incubated at 37 °C in a humidified atmosphere containing 5 % carbon dioxide. After 1 h, the cells were washed with cold D-PBS and stained for flow cytometry.

2.13. Isolation of mouse bone marrow neutrophils

Neutrophils were isolated from the bone marrow of healthy $Irf8^{+/+}$ mice and $Irf8^{-/-}$ mice and identified by flow cytometry using a BV650 anti-mouse Ly6g antibody. Neutrophils were resuspended in RPMI 1640 and seeded onto 24-well plates at 37 °C in a humidified atmosphere for 30 min before stimulation. The cells were incubated with 200 nM PMA (MCE, USA). After 3 h, the cells were collected for qRT−PCR or transwell chemotaxis assays, and the supernatant was collected for ELISA.

2.14. Ex vivo transwell chemotaxis assay

One day after AKI, kidney MPCs were isolated using a Percoll gradient under sterile conditions. Cell sorting was performed on a MA900 instrument (Sony, Japan). A total of 1×10^4 cDC1s, type 2 conventional dendritic cells (cDC2s), pDCs, moDCs or monocytes were individually added to the upper chamber of transwells (5-μm pore size, Costar, USA) in a 24-well plate containing 1 μM CCL-19 (Sino Biological, China) in the lower chamber. Neutrophils (2×10^5) from the bone marrow were added to the upper chamber of a transwell plate containing 50 nM fMLP (Sigma, USA). After 2–3 h, the cells in the lower chamber were collected, and the data were recorded using AccuCheck counting beads.

2.15. Statistical analysis

All the data are presented as the mean ± SD. The normality of the data was checked using the Shapiro−Wilk test. Statistical significance was calculated using a t-test, the Mann−Whitney test, or the Wilcoxon test. Multiple comparisons were performed using one-way ANOVA with Tukey's post hoc test for parametric data or two-way ANOVA with Dunnett's test for nonparametric data under the Bonferroni correction. R software (version 4.0.3) and GraphPad Prism 7 were utilized for statistical analysis. A p value < 0.05 was considered significant.

3. Results

3.1. The expression of IRF8 increases in patients and mice with AKI

To investigate the expression pattern of IRF8, we collected blood from patients with AKI and healthy individuals. To characterize human blood leukocytes, we used multiflow cytometric analysis as previously described [28]. Human blood moDCs were identified according to the expression of CD11c and HLA-DR within the $CD14^+$ monocyte population (Supplemental Fig. 1). Out of the $CD14^-$ cell population, following cell populations were identified: T cells ($CD3^+$), neutrophils ($CD3^-CD15^+$), B cells ($CD3^-CD15^-CD19^+$), and DCs ($CD14^-CD3^-HLA-DR^+CD11c^+$). The DCs were split into $CD123^+$ plasmacytoid dendritic cells (pDCs) and $CD123^-$ cells. Out of the $CD123^-$ cells, two populations of $CD123^-$ cells were identified: $CD141^+$ cDC1s and $CD1c^+$ cDC2s.

In healthy individuals, IRF8 was primarily expressed in blood cDC1s, pDCs, moDCs and monocytes (Fig. 1A), while in patients with AKI, the expression levels of IRF8 increased in cDC1s, moDCs, and monocytes when compared to that in healthy individuals (Fig. 1B, B'). However, the expression of IRF8 in blood pDCs and neutrophils significantly decreased, while that in blood cDC2s remained unaffected (Fig. 1B, B"). Moreover, we confirmed an increased accumulation of $IRF8^+$ cells (Fig. 1C and F) in the interstitium of kidney biopsies from patients with AKI, which were costained with $HLA-DR^+$ cells (Fig. 1E).

Additionally, we identified DCs in the kidney of healthy mice or mice after AKI as $CD45^+$ leukocytes by excluding $CD49^+$ NK cells, $CD3e^+$ T cells, $CD19^+$ B cells, and $Ly6g^+$ neutrophils (Supplemental Fig. 2A). Monocytes were gated by distinct expression levels of Ly6c and CD11b. The expression of CD64 and MHC II on $Ly6c^+CD11b^+$ monocytes was utilized to identify moDCs. The CD123, XCR1, and CD11b expression on $Ly6c^-$ cells was analyzed to identify $CD123^+$ pDCs, $XCR1^+$ cDC1s, and $CD11b^+$ cDC2s (Supplemental Fig. 2A). After IRI-induced AKI, we also observed an increase in the accumulation of $IRF8^+$ cells in the kidney interstitium (Fig. 1D). Flow cytometry confirmed that cDC1s, pDCs, moDCs, and monocytes in the kidney expressed IRF8 following IRI-induced AKI (Fig. 1G, Supplemental Fig. 1B). No difference in the expression of IRF8 was found in the cDC2s or neutrophils in the groups. Taken together, these data indicate that IRF8 expression is increased in immune cells during AKI.
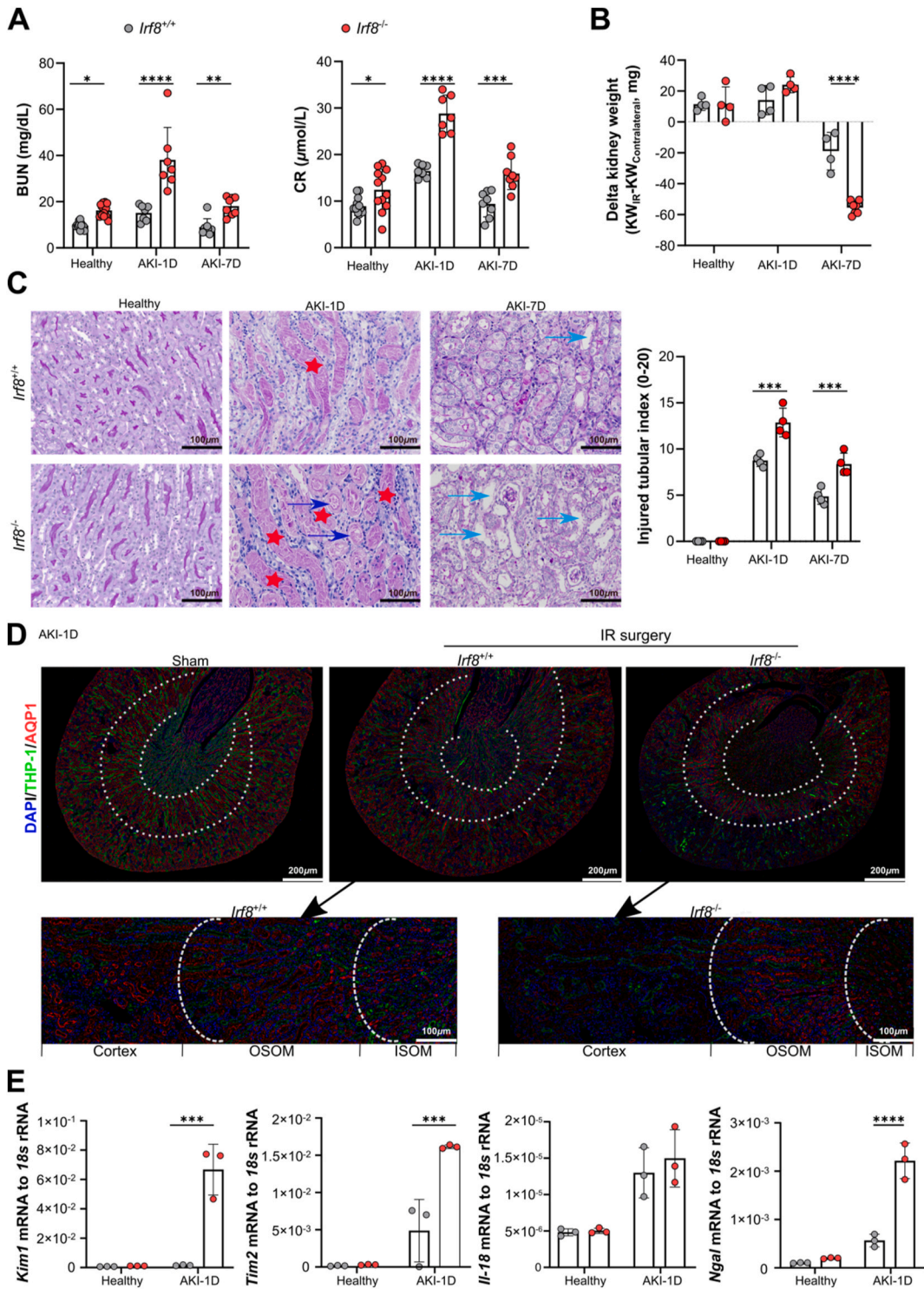
(caption on next page)

Fig. 2. *Irf8* deletion aggravates renal dysfunction during AKI. *Irf8*$^{+/+}$ and *Irf8*$^{-/-}$ mice were subjected to unilateral ischemic reperfusion (IR) surgery and sacrificed 1 day or 7 days after AKI. The healthy group represents mice that did not undergo IR surgery. (**A**) Blood urea nitrogen (BUN) levels and serum creatinine (CR) levels ($n \geq 3$ per group). (**B**) Weight loss in the kidneys of the IR group compared to that of the sham group was determined as follows: Delta kidney weight = KW$_{IR}$ – KW$_{contralateral}$ ($n \geq 3$ per group). (**C**) PAS-stained sections and tubular injury scores were evaluated in high-power fields ($n = 4$ per group). Scale bar, 100 μm. Red star: cast formation; Blue arrow: cell necrosis. Green arrow: tubular dilation. (**D**) The upper panel shows images of proximal tubules and distal tubules with immunolabeling for aquaporin-1 (AQP1, red) and Tamm-Horsfall protein-1 (THP-1, green) in the cortex, outer stripe of the outer medulla (OSOM), and inner stripe of the outer medulla (ISOM) (scale bar, 200 μm) from IR kidneys or sham kidneys on day 1 after AKI. Nuclei were counterstained with DAPI (blue). The bottom panel shows magnified IR kidney sections from *Irf8*$^{+/+}$ and *Irf8*$^{-/-}$ mice (scale bar, 100 μm). (**E**) The mRNA expression of tubular injury markers in the healthy group and AKI-1D group was normalized to *18S* rRNA expression ($n = 3$ per group). Each dot represents one mouse. The data are shown as the mean ± SD. *$p <$ 0.05, **$p < 0.01$, ***$p < 0.001$, and ****$p < 0.0001$. Two-way ANOVA. (For interpretation of the references to color in this figure legend, the reader is referred to the Web version of this article.)

3.2. Deletion of Irf8 aggravates renal dysfunction during AKI

In a recent study, we showed that in transgenic mice lacking *Irf8* in *Clec9a*-expressing cDC1s, kidney injury and inflammation are slightly aggravated during IRI-induced AKI [6]. Whether global deletion of *Irf8* has detrimental effects on other immune cells and the inflammatory response and therefore contributes to severe renal failure remains unknown. To address this question, we deleted *Irf8* in mice by targeting exons 3–6. Before that, we observed loss of the brush border, cast formation, cell necrosis (Fig. 2C) and increased accumulation of neutrophils (Fig. 4B) and monocytes (Supplemental Fig. 4B) in the kidneys of *Irf8*$^{+/+}$ mice, although there were no significant changes in the serum BUN or CR levels (Fig. 2A). Furthermore, serum BUN and CR levels were significantly elevated in *Irf8*$^{-/-}$ mice than in *Irf8*$^{+/+}$ mice following IRI-induced AKI (Fig. 2A). Seven days after AKI, the kidney weight of *Irf8*$^{-/-}$ mice was further reduced as compared to *Irf8*$^{+/+}$ mice (Fig. 2B) due to marked loss of brush border, cast formation, cell necrosis and tubular dilation, as indicated by PAS staining and an increase in the injured tubule index (Fig. 2C).

Consistently, fewer proximal tubules survived in the *Irf8*$^{-/-}$ mice than in WT mice, as indicated by the reduced accumulation of AQP1^{+} cells in the cortex (red, Fig. 2D). Increased mRNA expression levels of the kidney injury markers *Kim1*, *Tim2*, and *Ngal* were detected in kidneys of *Irf8*$^{-/-}$ mice 1 day after AKI (Fig. 2E), while no difference in the intrarenal mRNA expression of *Il-18* was observed between groups. These data suggest that IRF8 has a renoprotective effect during IRI-induced AKI.

3.3. Deletion of Irf8 influences the renal residence of immune cells in healthy mice

IRF8 has been reported to influence the development of leukocytes [13–17]. To investigate the effect of IRF8 on the diversity of resident leukocytes in the kidney und homeostatic condition, flow cytometry was carried out on kidneys from healthy *Irf8*$^{+/+}$ and *Irf8*$^{-/-}$ mice (Supplemental Figs. 2B–2H). Although we found no difference in the total number of leukocytes in the healthy kidney of *Irf8*$^{+/+}$ and *Irf8*$^{-/-}$ mice (Supplemental Fig. 2B), we observed a reduction in the number of cDC1s, Ly6c$^{high-int}$ moDCs and T cells, but an increase in the percentage and number of neutrophils and Ly6c^{int} monocytes in the kidney of healthy *Irf8*$^{-/-}$ mice compared with *Irf8*$^{+/+}$ mice (Supplemental Figs. 2B–2H). However, cDC2s, pDCs, B cells and NK cells remained unaffected. This suggested that IRF8 influences the renal resident pool of leukocytes, including DCs, monocytes and neutrophils, under homeostatic conditions.

3.4. Deletion of Irf8 reduces the infiltration of renal dendritic cells and monocyte-derived dendritic cells during AKI

We showed that the cell number and percentage of kidney cDC1s continually increased after AKI (Fig. 3A). To investigate the effect of *Irf8* deletion in AKI further, we performed in depth flow cytometry found that compared with *Irf8*$^{+/+}$ mice, there was a significant decrease in the number and frequency of kidney cDC1s in *Irf8*$^{-/-}$ mice, while we did not observe differences in kidney cDC2s or pDCs between groups after IRI (Fig. 3A, Supplemental Fig. 3A). We further examined the effect of *Irf8* deletion on renal moDC accumulation during AKI. moDCs were identified by coexpression of MHC II and CD64 among Ly6c^{+} monocytes (Supplemental Fig. 2A). Compared with those in *Irf8*$^{+/+}$ mice, the numbers and frequencies of renal Ly6c^{high} moDCs, Ly6c^{int} moDCs, and Ly6c^{low} moDCs in *Irf8*$^{-/-}$ mice were significantly lower (Fig. 3B, C, 3D, Supplemental Fig. 3B), suggesting that IRF8 may alter the recruitment of cDC1s and monocyte differentiation into moDCs following IRI-induced AKI.

3.5. Deletion of Irf8 triggers the recruitment of monocytes and neutrophils during AKI

To address the potential contribution of IRF8 to renal leukocyte recruitment, flow cytometry analysis was performed. Our data revealed greater renal infiltration of Ly6c^{+} monocytes in *Irf8*$^{-/-}$ mice than in *Irf8*$^{+/+}$ mice 1 day after AKI (Supplemental Fig. 4A). Increased accumulation of CD11b^{+} CCR2^{+} monocytes in *Irf8*$^{-/-}$ mice 1 day after AKI was confirmed by fluorescence microscopy (Supplemental Fig. 4B and 4B'). Within the Ly6c^{+} monocyte population in *Irf8*$^{-/-}$ mice, Ly6c^{high} monocytes were present in lower numbers in the kidney 1 day after AKI, while Ly6c^{int} and Ly6c^{low} monocytes infiltrated the kidney in greater numbers in *Irf8*$^{-/-}$ mice than in *Irf8*$^{+/+}$ mice (Supplemental Fig. 4C and 4C').

In addition, we observed greater infiltration of Ly6g^{+}CD11b^{+} neutrophils in the kidneys and spleens of *Irf8*$^{-/-}$ mice than in those of *Irf8*$^{+/+}$ mice 1 day after AKI (Fig. 4B, B', 4B″, Supplemental Fig. 3C). The Ly6g^{+} neutrophils were mainly distributed in the outer stripe outer medulla (OSOM) of the kidney and around the germinal center of the spleen in the *Irf8*$^{-/-}$ mice (Fig. 4C, C'). To confirm the *in*
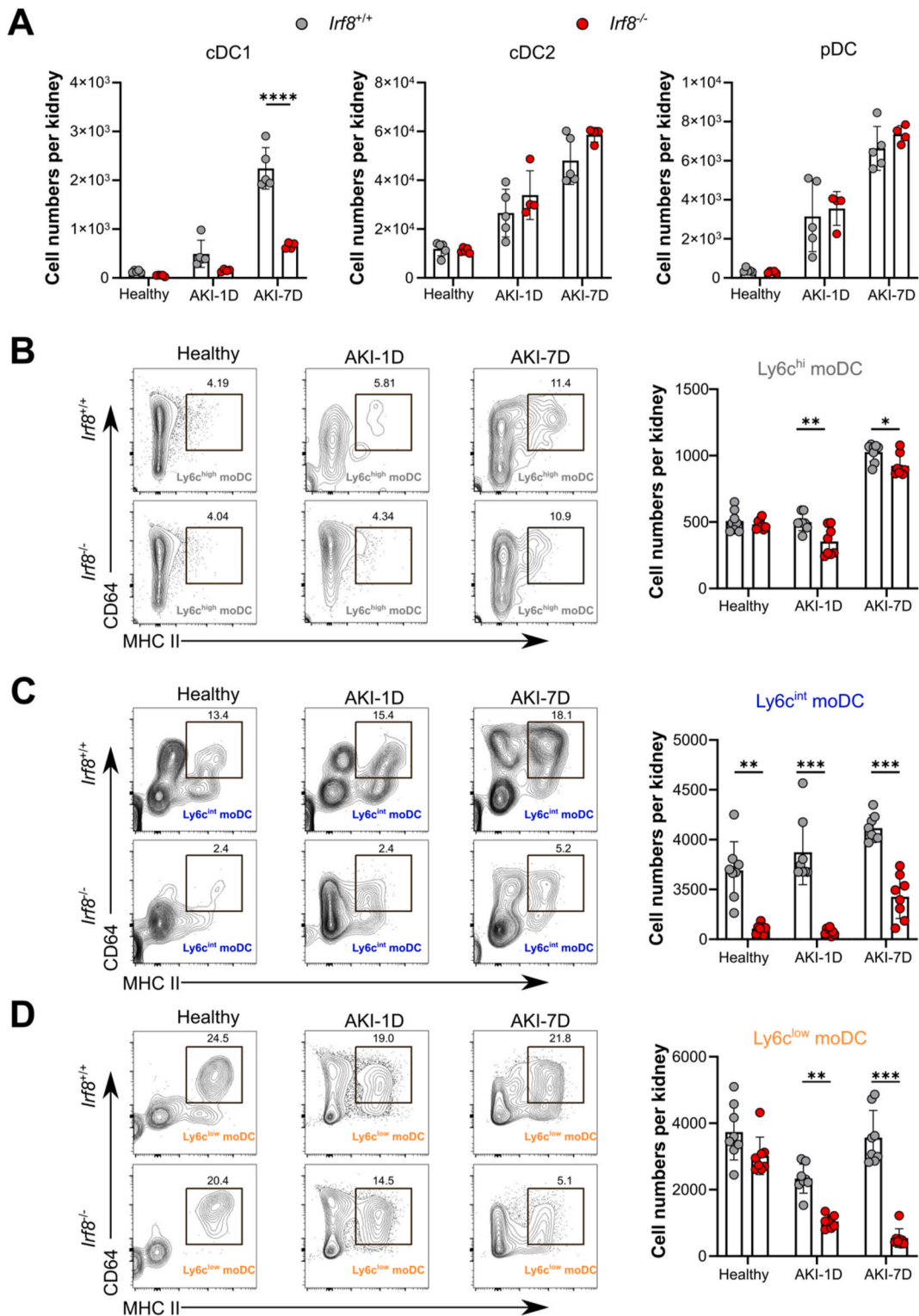
Fig. 3. *Irf8* deletion prevents type I conventional dendritic cell and monocyte-derived dendritic cell infiltration into the kidney during AKI. *Irf8*^{+/+} and *Irf8*^{−/−} mice were subjected to IR surgery. Kidney DCs were collected 1 day or 7 days after AKI and analyzed by flow cytometry according to the strategy illustrated in Supplemental Fig. 2A. (**A-D**) The absolute numbers of DCs in the kidney after AKI are shown ($n > 3$ mice per group). Each dot represents one mouse. The data are shown as the mean $\pm$ SD. *$p < 0.05$, **$p < 0.01$, ***$p < 0.001$, and ****$p < 0.0001$. Two-way ANOVA.
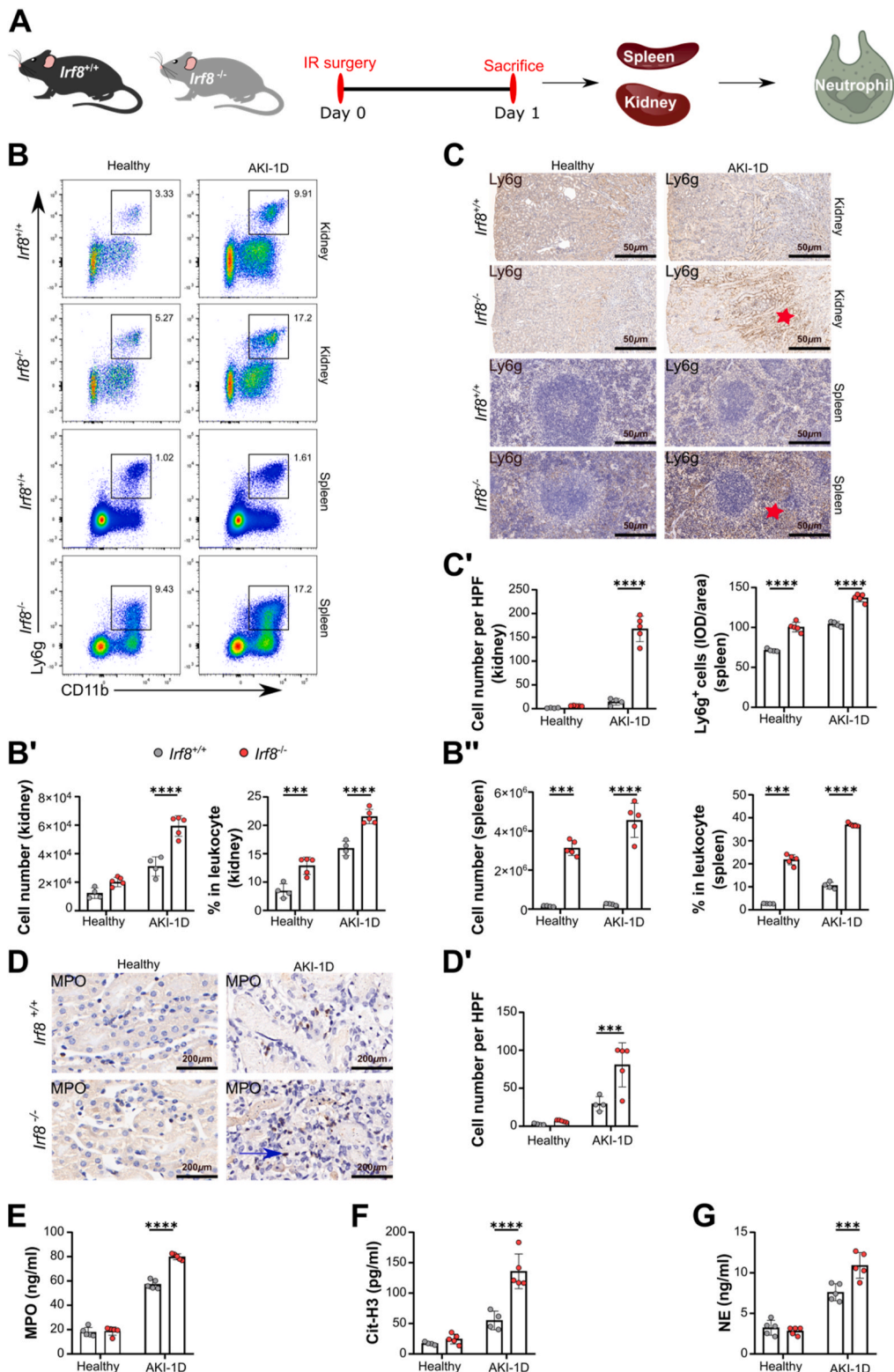
Fig. 4. *Irf8* deletion triggers neutrophil recruitment and NET formation during AKI. (**A**) Study design. *Irf8*^{+/+} and *Irf8*^{−/−} mice were subjected to IR surgery and sacrificed 1 day after AKI. The kidneys and spleens of mice were used for analysis. (**B**) Flow cytometric analysis of kidney and spleen neutrophils (CD45^{+}CD49^{−}CD3e^{−}CD19^{−}Ly6g^{+}CD11b^{+}, gated as indicated in Supplemental Fig. 2A). (**B′-B″**) The percentages and numbers of kidney/spleen neutrophils from healthy controls and mice after AKI (*n* = 4–5 mice per group). (**C–C′**) Distribution and cell numbers of Ly6g^{+} neutrophils in

kidneys and spleens ($n = 4–5$ mice per group) from healthy controls and mice after AKI. (**D**) Distribution of myeloperoxidase (MPO) in kidneys ($n = 4–5$ mice per group). Scale bar, 200 μm. (**D′**) Numbers of MPO$^+$ cells in kidneys. (**E-G**) Serum was collected from healthy and AKI mice, and the release of MPO, citrullinated histone 3 (Cit-H3), and neutrophil elastase (NE) was determined using ELISA kits ($n = 5$ mice per group). Each dot represents one mouse. Red star and blue arrow indicate positive cells. The data are shown as the mean ± SD. ***$p < 0.001$, ****$p < 0.0001$. Two-way ANOVA. (For interpretation of the references to color in this figure legend, the reader is referred to the Web version of this article.)

vivo data, we isolated bone marrow Ly6g$^+$ neutrophils from *Irf8*$^{+/+}$ and *Irf8*$^{-/-}$ mice and performed transwell migration assays (Fig. 5A and B). As shown in Fig. 5B, neutrophils isolated from *Irf8*$^{-/-}$ mice migrated more toward the chemoattractant fMLP than did neutrophils from *Irf8*$^{+/+}$ mice, suggesting that the loss of IRF8 augments integrin-mediated neutrophil migration.

Tissue injury and inflammation are also associated with NET formation, which leads to cell necrosis [26]. To determine the effect of IRF8 on NET formation, kidney histology was performed, and the serum levels of NET-related markers, including MPO, Cit-H3, and NE, were measured. Compared with those in *Irf8*$^{+/+}$ mice, *Irf8*$^{-/-}$ mice 1 day after AKI had increased levels of the granular protein MPO in both kidneys and serum (Fig. 4D, D', 4E), as well as increased serum levels of Cit-H3 and NE (Fig. 4F and G). Compared with those from *Irf8*$^{+/+}$ mice, bone marrow neutrophils isolated from *Irf8*$^{-/-}$ mice showed increased mRNA expression levels of *Mpo*, *Nfkb1*, and *Nox2* and increased release of Cit-H3, MPO, and NE upon *in vitro* activation with PMA (Fig. 5C and D). Taken together, these data indicate that *Irf8* deletion promotes the migration of neutrophils and NET formation in the kidney during AKI.
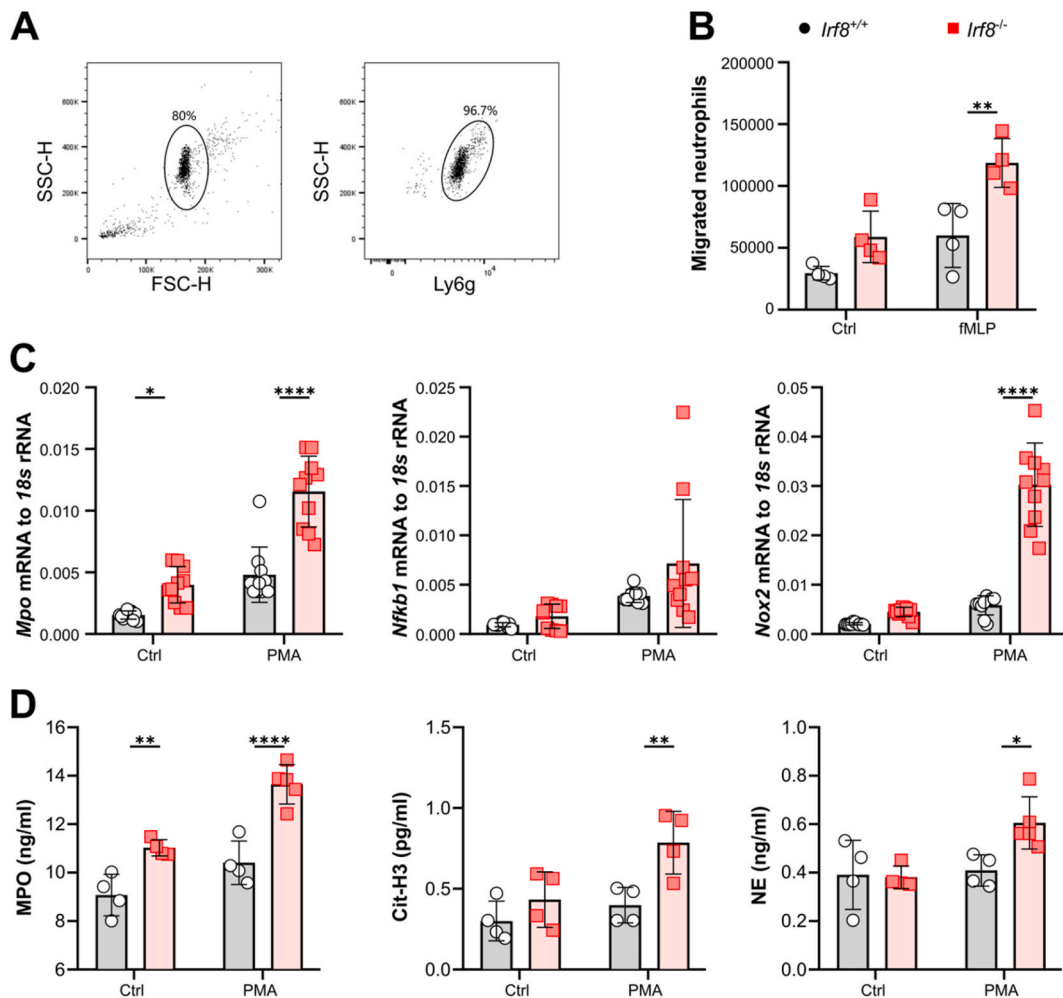

Fig. 5. *Irf8* deletion increases neutrophil migration *in vitro*. (**A**) Neutrophils were isolated from mouse bone marrow and identified as mature Ly6g$^+$ by flow cytometry with a purity of ~97 %. (**B**) The total number of neutrophils isolated from *Irf8*$^{+/+}$ and *Irf8*$^{-/-}$ mice that migrated toward the chemoattractant fMLP was determined by flow cytometry after 3 h ($n = 4$ mice per group). (**C**) mRNA expression of *Mpo*, *Nfkb1*, and *Nox2* in isolated neutrophils subjected to PMA incubation ($n \geq 5$ mice per group). (**D**) The release of Cit-H3, MPO, and NE by PMA-stimulated neutrophils was determined using ELISA kits ($n \geq 4$ mice per group). Each dot represents one mouse. The data are shown as the mean ± SD. *$p < 0.05$, **$p < 0.01$, and ****$p < 0.0001$. Two-way ANOVA. Ctrl, control.
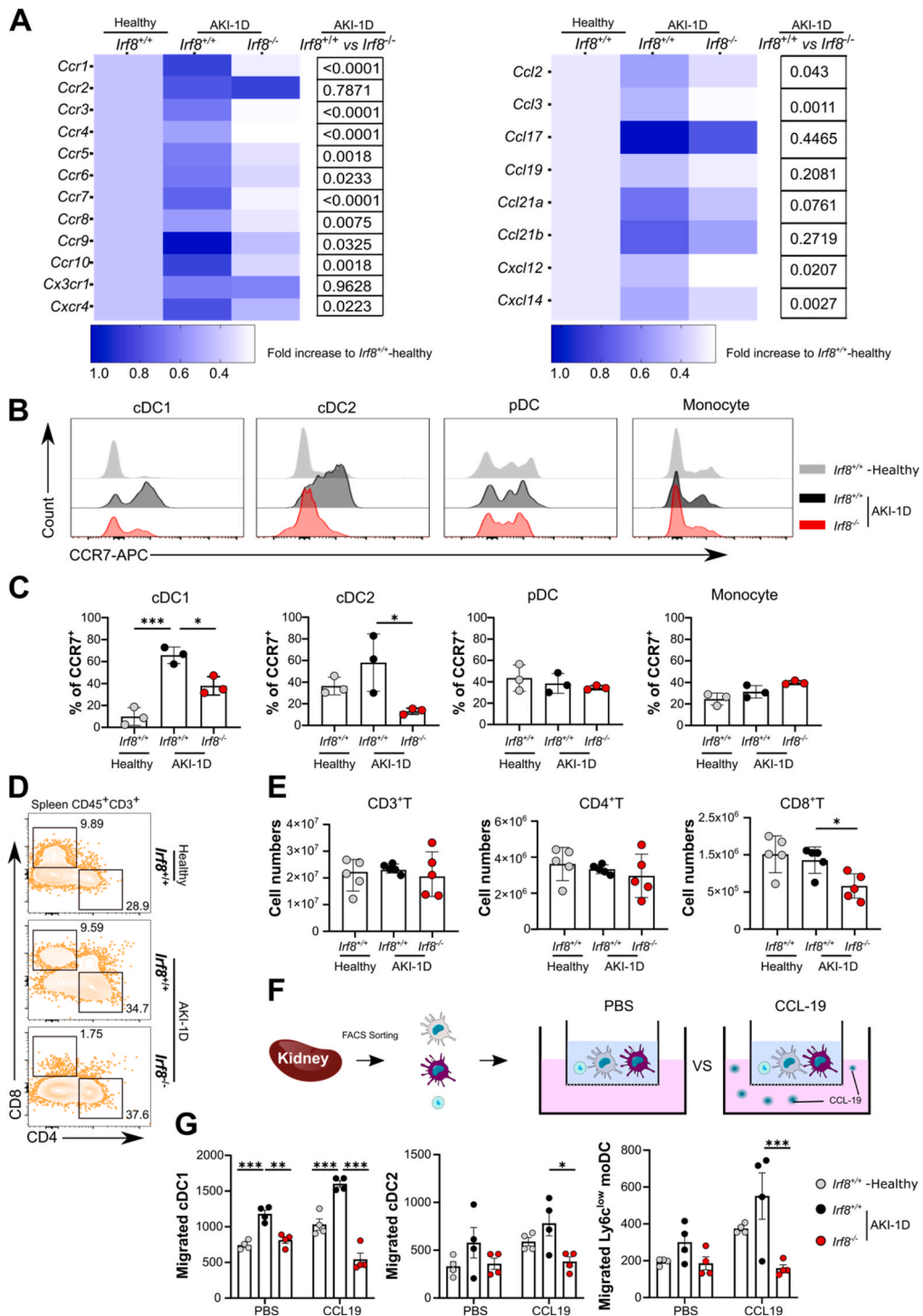
Fig. 6. *Irf8* deletion impairs DC trafficking and T-cell priming during AKI. *Irf8*$^{+/+}$ and *Irf8*$^{-/-}$ mice were subjected to IR surgery, and kidney MPCs were analyzed 1 day after AKI. (**A**) mRNA expression levels of genes encoding CC chemokine receptors (CCRs) and ligands (CCLs) in kidney MPCs were normalized to *18S* rRNA expression. The data are illustrated in heatmaps. The color intensity represents the mean expression value of each group. The *p* values for gene expression differences between the *Irf8*$^{+/+}$ and *Irf8*$^{-/-}$ groups 1 day after AKI were calculated. A *p* value < 0.05 was considered significant. $n = 3$–5 mice per group. (**B–C**) The expression of CCR7 in kidney MPCs was measured by flow cytometry. Kidneys were harvested from *Irf8*$^{+/+}$ (black) and *Irf8*$^{-/-}$ (red) mice 1 day after AKI and from healthy *Irf8*$^{+/+}$ mice (gray). Images from three independent experiments and the percentages of CCR7^{+} cells among each kidney MPC are shown. $n = 3$ mice per group. (**D**) Splenic T-cell subsets (gated on CD45^{+}CD19^{-}CD3e^{+} T cells, Supplemental Fig. 2A). (**E**) Absolute numbers of splenic CD3^{+} T cells, CD4^{+} T cells, and CD8^{+} T cells. $n = 5$–6 mice per

group. (**F**) Kidney MPCs were isolated 1 day after AKI, and each DC subset was sorted for *in vitro* Transwell migration assays. (**G**) The total number of each DC subset that migrated toward the CCL-19 stimulus was quantified. $n = 4$ mice per group. Each dot represents one mouse. The data are shown as the mean $\pm$ SD. $*p < 0.05$, $**p < 0.01$, and $***p < 0.001$. *t*-test, one-way ANOVA or two-way ANOVA. (For interpretation of the references to color in this figure legend, the reader is referred to the Web version of this article.)

3.6. Deletion of Irf8 inhibits the maturation of dendritic cells during AKI

DCs require IRF8 for their maturation, activation, and differentiation during viral infections; these mechanisms are important for antigen presentation [29]. To investigate this phenomenon in AKI, we performed extensive flow cytometry analysis of kidney DC subpopulations and found that 1 day after AKI, kidney cDC1s from $Irf8^{-/-}$ mice showed no or lower expression of the maturation markers CD40, MHC II, and CD11c compared with those from $Irf8^{+/+}$ mice (Supplemental Fig. 5A, 1st line). Compared with those from the $Irf8^{+/+}$ mice, the cDC2s from $Irf8^{-/-}$ mice expressed lower levels of CD40, CD86, and CD11c (Supplemental Fig. 5A, 2nd line), similar to the CD40, CD86, and MHC II expression of pDCs from the $Irf8^{-/-}$ mice (Supplemental Fig. 5A, 3rd line). Additionally,
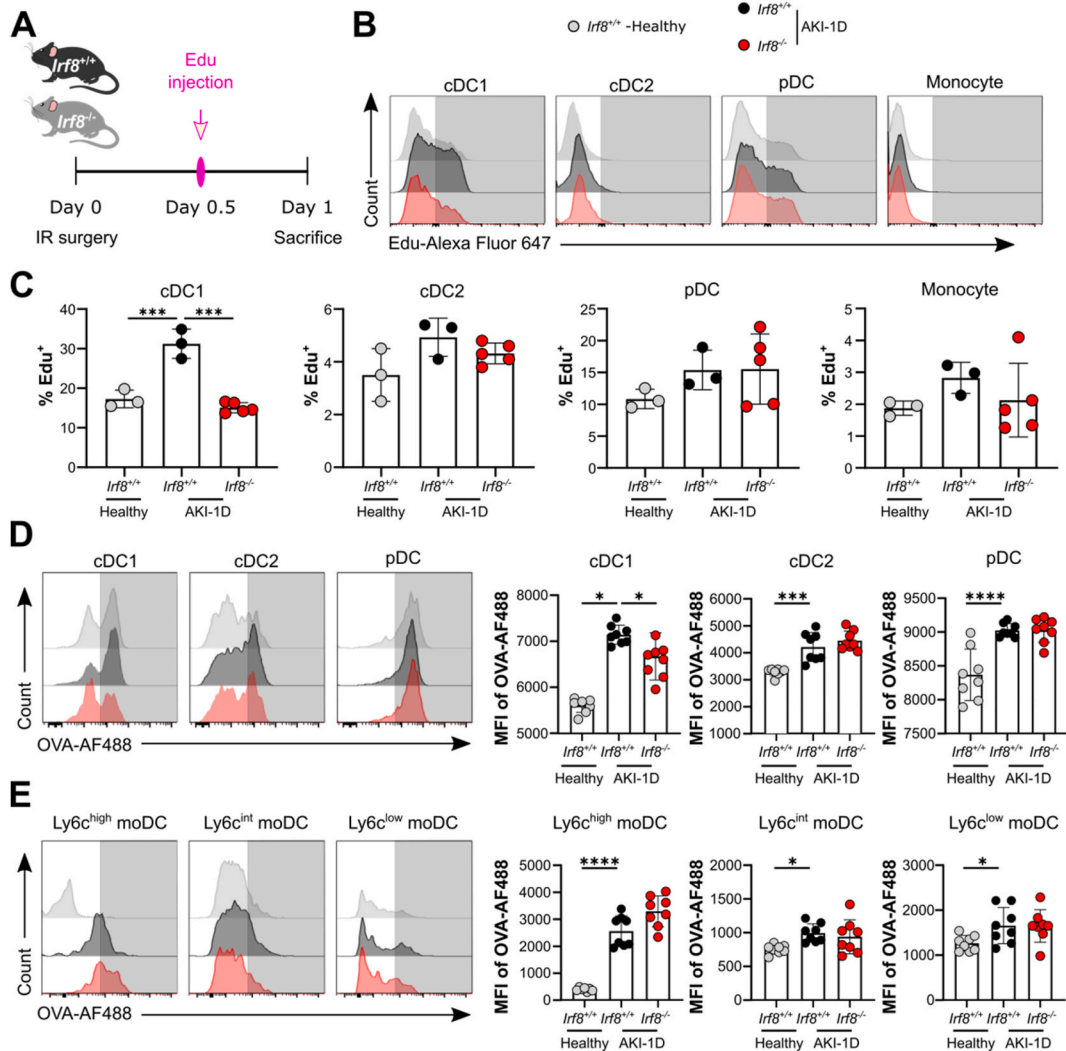

Fig. 7. *Irf8* deletion impairs the proliferation and antigen uptake of kidney DCs during AKI. (**A**) Experimental design. Twelve hours after IR surgery, EdU was injected i.p. 12 h before the mice were sacrificed. (**B**) Histogram plots showing EdU incorporation in kidney MPCs from $Irf8^{+/+}$ (black) or $Irf8^{-/-}$ (red) mice 1 day after AKI and from healthy $Irf8^{+/+}$ mice (gray). Representative images of three independent experiments are shown. (**C**) Percentages of EdU-positive cells in each MPC subset ($n = 3$–5 mice per group). (**D-E**) Flow cytometry analysis of antigen uptake by kidney MPCs. Kidneys were harvested from AKI mice and healthy mice. MPCs freshly isolated from kidneys were exposed to ovalbumin-Alexa Fluor 488 (OVA-AF488). Antigen incorporation was visualized by calculating the mean fluorescence intensity (MFI) of OVA-AF488 in each subset ($n > 3$ mice per group). The data are shown as the mean $\pm$ SD. $*p < 0.05$, $***p < 0.001$, and $****p < 0.0001$. One-way ANOVA. (For interpretation of the references to color in this figure legend, the reader is referred to the Web version of this article.)

Ly6c^{high} and Ly6c^{low} moDCs from *Irf8*$^{-/-}$ mice had lower expression of CD40 and CD11c, respectively, as well as CD40, MHC II, and CD11c, than did those from *Irf8*$^{+/+}$ mice, while all the other markers were expressed at lower levels in Ly6c^{int} moDCs from *Irf8*$^{-/-}$ mice (Supplemental Fig. 5A, 4th-6th lines). This finding suggested that IRF8 regulates the maturation, activation, and differentiation of renal DCs during AKI.

3.7. Deletion of Irf8 impairs dendritic cell trafficking and T-cell priming during AKI

We next asked whether IRF8 affects the expression of chemokine receptors in monocytes and DCs during IRI-induced AKI. To answer this question, kidney MPCs were isolated for qRT–PCR analysis (Fig. 6A). The mRNA expression levels of the chemokine receptors *Ccr1, Ccr3, Ccr4, Ccr5, Ccr6, Ccr7, Ccr8, Ccr9, Ccr10,* and *Cxcr4* were significantly lower in kidney MPCs from *Irf8*$^{-/-}$ mice than in those from *Irf8*$^{+/+}$ mice 1 day after IRI (Fig. 6A). However, the expression levels of *Cx3cr1*, which is a kidney-specific homing receptor for DCs, were similar between groups. We also found reduced renal expression of the ligands of CCRs (CCLs) *Ccl2, Ccl3, Cxcl12,* and *Cxcl14* in *Irf8*$^{-/-}$ mice, as indicated by the heatmap (Fig. 6A). In *Irf8*$^{+/+}$ mice, the percentages of CCR7^{+} cDC1s and CCR7^{+} cDC2s increased after AKI compared with those in healthy mice (Fig. 6B and C); there was a significant decrease in the number of these cells in *Irf8*$^{-/-}$ mice after AKI. No differences in CCR7^{+} pDCs, CCR7^{+} monocytes (Fig. 6B and C), or CCR7^{+} moDCs (data not shown) were observed between groups.

Mature DCs require CCRs to migrate to the kidney-draining lymph node and spleen, where they prime T cells and promote T-cell survival [23]. In the context of AKI, we found that the numbers of splenic CD4^{+} and CD8^{+} T cells were similar between healthy and ischemic *Irf8*$^{+/+}$ mice (Fig. 6D and E). However, the number of splenic CD8^{+} T cells was lower in *Irf8*$^{-/-}$ mice than in *Irf8*$^{+/+}$ mice 1 day after AKI (Fig. 6E). In addition, we performed *in vitro* transwell migration assays with renal cDC1s, cDC2s and Ly6c^{low} moDCs isolated from *Irf8*$^{+/+}$ and *Irf8*$^{-/-}$ mice (Fig. 6F) and found that all three cell populations were significantly less able to migrate toward the CCR7 ligand CCL-19 (Fig. 6G). An impaired migratory capability was not observed for kidney pDCs, Ly6c^{high} moDCs, or Ly6c^{int} moDCs from *Irf8*$^{-/-}$ mice (data not shown). Taken together, these data indicate that IRF8 regulates the trafficking of kidney DC subsets into the spleen for CD8^{+} T-cell priming during AKI.

3.8. Impaired Proliferation and antigen uptake of DCs in Irf8$^{-/-}$ Mice during AKI

Finally, we investigated the effect of IRF8 on DC proliferation and antigen uptake during AKI. For this experiment, *Irf8*$^{+/+}$ and *Irf8*$^{-/-}$ mice were injected with the thymidine analog EdU 12 h after IR surgery, and the percentages of proliferating EdU^{+} DCs and monocytes in the kidney were quantified by flow cytometry 24 h after surgery (Fig. 7A). *In vivo* pulse labeling of proliferating cells revealed an increase in proliferating DCs and monocytes in mice with AKI compared with healthy controls (Fig. 7B and C). Interestingly, renal cDC1s from *Irf8*$^{-/-}$ mice were significantly less able to proliferate than those from *Irf8*$^{+/+}$ mice after IRI-induced AKI (Fig. 7B and C). However, cDC2s, pDCs, monocytes, and moDCs from *Irf8*$^{-/-}$ mice showed normal EdU incorporation similar to that observed in *Irf8*$^{+/+}$ mice (Fig. 7B and C; moDCs are not shown), indicating that IRF8 affects only the proliferative capability of renal cDC1s during AKI.

To quantify the uptake of OVA antigen by kidney DCs, we harvested kidneys from *Irf8*$^{+/+}$ and *Irf8*$^{-/-}$ mice or from healthy mice 1 day after AKI and incubated the cells with OVA-AF488 for an additional 3 h. Our data revealed that all DC and moDC subsets from *Irf8*$^{+/+}$ mice showed increased uptake of OVA antigen after AKI compared with those in the healthy group, as indicated by the increased mean fluorescence intensity (MFI) of OVA-AF488 (Fig. 7D and E). In accordance with the reduced proliferative capability of cDC1s (Fig. 7B and C), cDC1s from *Irf8*$^{-/-}$ mice showed significantly reduced uptake of the OVA antigen compared with those from the *Irf8*$^{+/+}$ mice 1 day after AKI, while the uptake of OVA by the cDC2s, pDCs, and moDCs did not differ between the *Irf8*$^{+/+}$ and *Irf8*$^{-/-}$ mice (Fig. 7D and E). Additionally, the intrarenal mRNA expression levels of *Ifn-α7, Ifn-γ,* and *Ifn-κ* were significantly lower in *Irf8*$^{-/-}$ mice than in *Irf8*$^{+/+}$ mice during AKI (Supplemental Fig. 5B), which indicates that IFN production is lower in mice with *Irf8* deletion. Taken together, our results demonstrate that IRF8 regulates the proliferative and antigen-presenting capabilities of renal cDC1s following tissue injury and inflammation.

4. Discussion

We hypothesized that IRF8 can modulate the recruitment of several types of leukocytes, their differentiation state, and their function during the early phase of IRI-induced AKI, which subsequently alleviates kidney injury and inflammation. Our data showed that *Irf8* deficiency reduces the infiltration of cDC1s and moDCs into ischemic kidneys but increases neutrophil migration and NET formation following IRI-induced AKI. In addition, we found that global *Irf8* deficiency impaired DC maturation and activation, and specifically cDC1 proliferation, antigen uptake, and trafficking to lymphoid organs for T-cell priming. These results showed that IRF8 primarily regulates cDC1s and affects neutrophil functions, thereby protecting mice from kidney injury and inflammation following IRI.

The enhancers required for cDC1 development are manifested at different developmental stages [31]. DCs are derived from MDPs, which give rise to common dendritic cell progenitors (CDPs), leading to the production of distinct clonogenic progenitors: pre-cDC1s and pre-cDC2s. Studies have shown that the +32 kilobase (kb) *Irf8* enhancer is active only after cDC1 specification and remains active in fully developed cDC1s, whereas the +41 kb *Irf8* enhancer is required for the specification of pre-cDC1s from CDPs [30,31]. Phenotypically, cDC1s in *Irf8*$^{+32-/-}$ and *Irf8*$^{+41-/-}$ mice were selectively absent in all tissues, and functional defects were restricted to this lineage [32], while leukocytes in *Irf8*$^{-50-/-}$ mice were normal but showed reduced intracellular IRF8 protein levels [32]. We

generated a targeted deletion of exons 3–6 from the *Irf8* transcriptional start site (TSS) [27], which is located at sites upstream of +32 kb and +41 kb but is residual in renal cDC1s. On the one hand, the existence of +32 kb, +41 kb, or other unknown enhancers, accounts for cDC1 specification and development. On the other hand, Baft3 binding to the *Irf8* TSS can compensate for the loss of *Irf8* during cDC1 development. Our mouse model may help elucidate the mechanisms that control the differences in fate that are still not fully understood.

DCs take up antigens (including molecules released by necrotic cells) via endocytosis for processing and MHC II-mediated antigen presentation to naive T cells [12]. Studies have demonstrated that IRF8 can directly regulate cytoskeleton-related and endosomal/lysozomal enzyme-related genes that are important for antigen processing and MHC II molecule targeting [33]. ICSBP$^{-/-}$ CD8α^+ DCs (namely, cDC1s) lack endocytic activity [13]. Splenic CD8α^- DCs (namely, cDC2s) exhibit increased MHC II-mediated presentation of exogenous antigens, whereas CD8α^+ DCs specialize in cell-associated antigen presentation [18,34]. Consistently, we observed defective activation and maturation of *Irf8*$^{-/-}$ cDC1s in AKI due to the inability of *Irf8*$^{-/-}$ cDC1s to take up OVA peptide and reduced MHC II expression, which explains the impaired T-cell proliferation in the spleen during AKI. T-cell proliferation depends on the maturation stage of DCs during AKI [5]. We showed that the expression of the maturation marker CD40 is reduced in *Irf8*$^{-/-}$ cDC1s in IRI-induced AKI, which is in line with previous data showing that IRF8 enhances the expression of CD40 upon TLR9 signaling in DCs [35].

IRF8 is known to regulate cDC1 development by controlling the differentiation of CDPs to pre-cDC1s in the bone marrow [14,17]. IRF8 is also responsible for maintaining a high proportion of terminally differentiated cDC1s to prevent their conversion into cDC2s [29]. This finding is consistent with our findings showing that the expression of IRF in blood cDC1s is greater than that in cDC2s in healthy individuals. Interestingly, the expression of IRF8 in circulating cDC1s also significantly increases in patients with AKI, while that on circulating cDC2s remains unaffected. Using mice with global *Irf8* deficiency and *in vitro* transwell migration assays, we confirmed that *Irf8* deletion inhibits the migration and differentiation of cDC1s. This inhibition could be due to reduced CCR7, CCR9 and CCL21a expression in *Irf8*$^{-/-}$ cDC1s because evidence suggests that CCR7/CCL19/CCL21 promotes DC migration to protect against sepsis-induced AKI [31].

While IRF8 is critical for pDC development in the bone marrow [36–38] and pDCs are important for IFN-α/β secretion in viral infections and systemic lupus erythematosus [39,40], our results indicated that IRF8 is most likely not involved in pDC survival and migration during AKI. Although MHC II expression in *Irf8*$^{-/-}$ pDCs was not altered, we were unable to determine if IRF8 was not responsible for MHC II expression on pDCs due to the compensatory role of IRF4 [41]. Thus, further investigations are needed to elucidate the potential link between IRF8 and pDCs in disease.

The effect of IRF8 on renal monocytes (identified as Ly6c$^+$ cells [41]) is poorly understood. Ly6c^{high} monocytes originate from MDPs, which express high levels of IRF8 [17]. Healthy mice deficient in *Irf8* have reduced numbers of Ly6c$^+$ monocytes in the bone marrow, blood, and spleen [42]. Our data confirmed that healthy *Irf8*$^{-/-}$ mice showed less infiltration of Ly6c^{high} monocytes into the kidneys (Supplemental Fig. 2D, although $p = 0.34$ [*Irf8*$^{+/+}$ *vs. Irf8*$^{-/-}$]), suggesting that IRF8 is necessary for the development and recruitment of renal Ly6c^{high} monocytes. However, the number of kidney Ly6c^{int} monocytes that display anti-inflammatory and reparative properties [41] is lower than that of Ly6c^{high} monocytes in *Irf8*$^{-/-}$ mice [43]. Moreover, we found that Ly6c^{int} monocytes accumulated in high numbers in healthy and injured kidneys despite the reduced accumulation of Ly6c^{high} monocytes in *Irf8*$^{-/-}$ mice. One possible explanation is that IRF8 affects the differentiation of Ly6c^{int} monocytes into Ly6c^{high} monocytes or that increased tissue damage triggers a counterbalance in Ly6c^{int} monocytes [44–46]. The reduced accumulation of Ly6c^{high} monocytes may account for the lower number of moDCs in *Irf8*$^{-/-}$ kidneys during AKI because Ly6c^{high} monocytes are known to differentiate into moDCs [46–48]. Thus, IRF8 may contribute to the heterogeneity of monocytes and moDCs and their functional phenotype during tissue injury, similar to the regulatory effects of IRF4 [49]. Whether IRF8 specifically affects the development and functions of Ly6c^{high} monocytes and moDCs in AKI needs to be addressed in future experiments using cell-specific transgenic mouse models.

Moreover, AKI is also characterized by the extensive infiltration of neutrophils and NET formation, which contribute to necroinflammation [50–52]. IRF8 is only low expressed in neutrophils which in turn may disrupts the hematopoiesis of neutrophils by interacting with C/EBPα and by activating KLF4 [19,20,53,54]. Consistently, we found that there were more neutrophils in the kidney and spleen of healthy *Irf8*$^{-/-}$ mice than in those of *Irf8*$^{+/+}$ mice, and these numbers further increased upon IRI-induced AKI. *Irf8* deficiency promotes not only the recruitment of neutrophils into the ischemic kidney but also their ability to form NETs, suggesting that IRF8 indirectly affects neutrophil recruitment and function. Additionally, the loss of cDC1s may counterbalance the recruitment of neutrophils [6].

In summary, our study indicated that IRF8 protects mice against IRI-induced AKI by controlling the function of cDC1s and moDCs, and by regulating neutrophil recruitment and NET formation. Thus, our detailed characterization of mice with global *Irf8* deficiency provides a deeper mechanistic understanding of the role of IRF8 in DCs and their functional phenotype during AKI and beyond.

Ethical approval

This study was reviewed and approved by the Ethics Committee of the Seventh Affiliated Hospital of Sun Yat-Sen University (KY-2022-025-02, KY-2023-081-01). All participant provided informed consent to participate in the study and that for the publication of their anonymised case details and images.

All animal experiments were approved by the Animal Care and Use Committee of Sun Yat-Sen University (SYSU-IACUC-2022-B1127).

Data availability statement

Data will be made available on request (DOI 10.17605/OSF.IO/VK7U8, shared on OSF website).

CRediT authorship contribution statement

Na Li: Writing – original draft, Conceptualization. **Stefanie Steiger:** Writing – review & editing. **Ming Zhong:** Data curation. **Meihua Lu:** Data curation. **Yan Lei:** Data curation. **Chun Tang:** Data curation. **Jiasi Chen:** Data curation. **Yao Guo:** Data curation. **Jinhong Li:** Data curation. **Dengyang Zhang:** Data curation. **Jingyi Li:** Data curation. **Enyi Zhu:** Data curation. **Zhihua Zheng:** Investigation. **Julia Lichtnekert:** Conceptualization. **Yun Chen:** Conceptualization. **Xiaohua Wang:** Conceptualization.

Declaration of competing interest

The authors declare that they have no known competing financial interests or personal relationships that could have appeared to influence the work reported in this paper.

Appendix A. Supplementary data

Supplementary data to this article can be found online at https://doi.org/10.1016/j.heliyon.2024.e31818.

References

[1] A.A. Sharfuddin, B.A. Molitoris, Pathophysiology of ischemic acute kidney injury, Nature reviews. Nat Rev Nephrol. 7 (2011) 189–200.

[2] M. Sekine, T. Monkawa, R. Morizane, K. Matsuoka, C. Taya, Y. Akita, K. Joh, H. Itoh, M. Hayashi, Y. Kikkawa, C. Kohno, A. Suzuki, H. Yonekawa, Selective depletion of mouse kidney proximal straight tubule cells causes acute kidney injury, Transgenic Res. 21 (2012) 51–62.

[3] S.R. Mulay, A. Linkermann, H.J. Anders, Necroinflammation in kidney disease, JASN (J. Am. Soc. Nephrol.) 27 (2016) 27–39.

[4] X. Dong, S. Swaminathan, L.A. Bachman, A.J. Croatt, K.A. Nath, M.D. Griffin, Resident dendritic cells are the predominant TNF-secreting cell in early renal ischemia-reperfusion injury, Kidney Int. 71 (2007) 619–628.

[5] C. Kurts, F. Ginhoux, U. Panzer, Kidney dendritic cells: fundamental biology and functional roles in health and disease, Nat. Rev. Nephrol. 16 (2020) 391–407.

[6] N. Li, S. Steiger, L. Fei, C. Li, C. Shi, N. Salei, B.U. Schraml, Z. Zheng, H.J. Anders, J. Lichtnekert, IRF8-Dependent type I conventional dendritic cells (cDC1s) control post-ischemic inflammation and mildly protect against post-ischemic acute kidney injury and disease, Front. Immunol. 12 (2021) 685559.

[7] N. Salei, S. Rambichler, J. Salvermoser, N.E. Papaioannou, R. Schuchert, D. Pakalniškytė, N. Li, J.A. Marschner, J. Lichtnekert, C. Stremmel, F.M. Cernilogar, M. Salvermoser, B. Walzog, T. Straub, G. Schotta, H.J. Anders, C. Schulz, B.U. Schraml, The kidney contains ontogenetically distinct dendritic cell and macrophage subtypes throughout development that differ in their inflammatory properties, JASN (J. Am. Soc. Nephrol.) 31 (2020) 257–278.

[8] B.R. Sahoo, Structure of fish Toll-like receptors (TLR) and NOD-like receptors (NLR), Int. J. Biol. Macromol. 161 (2020) 1602–1617.

[9] M. Mojzesz, K. Rakus, M. Chadzinska, K. Nakagami, G. Biswas, M. Sakai, J.I. Hikima, Cytosolic sensors for pathogenic viral and bacterial nucleic acids in fish, Int. J. Mol. Sci. 21 (2020) 7289.

[10] G.N. Zhao, D.S. Jiang, H. Li, Interferon regulatory factors: at the crossroads of immunity, metabolism, and disease, Biochim. Biophys. Acta 1852 (2015) 365–378.

[11] A. Yáñez, H.S. Goodridge, Interferon regulatory factor 8 and the regulation of neutrophil, monocyte, and dendritic cell production, Curr. Opin. Hematol. 23 (2016) 11–17.

[12] D. Kurotaki, M. Yamamoto, A. Nishiyama, K. Uno, T. Ban, M. Ichino, H. Sasaki, S. Matsunaga, M. Yoshinari, A. Ryo, M. Nakazawa, K. Ozato, T. Tamura, IRF8 inhibits C/EBPα activity to restrain mononuclear phagocyte progenitors from differentiating into neutrophils, Nat. Commun. 5 (2014) 4978.

[13] U. Cytlak, A. Resteu, S. Pagan, K. Green, P. Milne, D. Maisuria, G. McDonald, A. Filby, B. Carpenter, R. Queen, S. Hambleton, R. Hague, H. Lango Allen, J.E.D. Thaventhiran, G. Doody, M. Collin, V. Bigley, Differential IRF8 transcription factor requirement defines two pathways of dendritic cell development in humans, Immunity 53 (2020) 353–370.e8.

[14] J. Schönheit, C. Kuhl, M.L. Gebhardt, F.F. Klett, P. Riemke, M. Scheller, G. Huang, R. Naumann, A. Leutz, C. Stocking, J. Priller, M.A. Andrade-Navarro, F. Rosenbauer, PU.1 level-directed chromatin structure remodeling at the Irf8 gene drives dendritic cell commitment, Cell Rep. 3 (2013) 1617–1628.

[15] T. Yashiro, M. Yamamoto, S. Araumi, et al., PU.1 and IRF8 modulate activation of NLRP3 inflammasome via regulating its expression in human macrophages, Front. Immunol. 12 (2021) 649572, https://doi.org/10.3389/fimmu.2021.649572. Published 2021 Apr 7.

[16] D. Sichien, C.L. Scott, L. Martens, M. Vanderkerken, S. Van Gassen, M. Plantinga, T. Joeris, S. De Prijck, L. Vanhoutte, M. Vanheerswynghels, G. Van Isterdael, W. Toussaint, F.B. Madeira, K. Vergote, W.W. Agace, B.E. Clausen, H. Hammad, M. Dalod, Y. Saeys, B.N. Lambrecht, M. Guilliams, IRF8 transcription factor controls survival and function of terminally differentiated conventional and plasmacytoid dendritic cells, respectively, Immunity 45 (2016) 626–640.

[17] Z. Cao, K.A. Budinich, H. Huang, D. Ren, B. Lu, Z. Zhang, Q. Chen, Y. Zhou, Y.H. Huang, F. Alikarami, M.C. Kingsley, A.K. Lenard, A. Wakabayashi, E. Khandros, W. Bailis, J. Qi, M.P. Carroll, G.A. Blobel, R.B. Faryabi, K.M. Bernt, J. Shi, ZMYND8-regulated IRF8 transcription axis is an acute myeloid leukemia dependency, Mol Cell 81 (2021) 3604–3622.e10.

[18] J.W. Lee, H.S. Kim, S. Kim, J. Hwang, Y.H. Kim, G.Y. Lim, W.J. Sohn, S.R. Yoon, J.Y. Kim, T.S. Park, K.M. Park, Z.Y. Ryoo, S. Lee, DACH1 regulates cell cycle progression of myeloid cells through the control of cyclin D, Cdk 4/6 and p21Cip1, Biochem. Biophys. Res. Commun. 420 (2012) 91–95.

[19] J.B. Lingrel, R. Pilcher-Roberts, J.E. Basford, P. Manoharan, J. Neumann, E.S. Konaniah, R. Srinivasan, V.Y. Bogdanov, D.Y. Hui, Myeloid-specific Krüppel-like factor 2 inactivation increases macrophage and neutrophil adhesion and promotes atherosclerosis, Circ. Res. 110 (2012) 1294–1302.

[20] H.J. de Heer, H. Hammad, T. Soullié, D. Hijdra, N. Vos, M.A. Willart, H.C. Hoogsteden, B.N. Lambrecht, Essential role of lung plasmacytoid dendritic cells in preventing asthmatic reactions to harmless inhaled antigen, J. Exp. Med. 200 (2004) 89–98.

[21] A. Das, K.S. Chauhan, H. Kumar, P. Tailor, Mutation in Irf8 gene (Irf8R294C) impairs type I IFN-mediated antiviral immune response by murine pDCs, Front. Immunol. 12 (2021) 758190.

[22] S. Salem, D. Salem, P. Gros, Role of IRF8 in immune cells functions, protection against infections, and susceptibility to inflammatory diseases, Hum. Genet. 139 (2020) 707–721.

[23] E. Lazzeri, M.L. Angelotti, A. Peired, C. Conte, J.A. Marschner, L. Maggi, B. Mazzinghi, D. Lombardi, M.E. Melica, S. Nardi, E. Ronconi, A. Sisti, G. Antonelli, F. Becherucci, L. De Chiara, R.R. Guevara, A. Burger, B. Schaefer, F. Annunziato, H.J. Anders, P. Romagnani, Endocycle-related tubular cell hypertrophy and progenitor proliferation recover renal function after acute kidney injury, Nat. Commun. 9 (2018) 1344.

[24] L.S. Chawla, P.L. Kimmel, Acute kidney injury and chronic kidney disease: an integrated clinical syndrome, Kidney Int. 82 (2012) 516–524.

[25] Q. Ma, R. Immler, M. Pruenster, M. Sellmayr, C. Li, A. von Brunn, B. von Brunn, R. Ehmann, R. Wölfel, M. Napoli, Q. Li, P. Romagnani, R.T. Böttcher, M. Sperandio, H.J. Anders, S. Steiger, Soluble uric acid inhibits β2 integrin-mediated neutrophil recruitment in innate immunity, Blood 23 (2022) 3402–3417.

[26] J. Feng, H. Wang, D.M. Shin, M. Masiuk, C.F. Qi, H.C. Morse, IFN regulatory factor 8 restricts the size of the marginal zone and follicular B cell pools, J. Immunol. 186 (3) (2011) 1458–1466.

[27] J.A. Marschner, H. Schäfer, A. Holderied, H.J. Anders, Optimizing mouse surgery with online rectal temperature monitoring and preoperative heat supply. Effects on post-ischemic acute kidney injury, PLoS One 11 (2016) e0149489.

[28] Y. Minoda, I. Virshup, I. Leal Rojas, O. Haigh, Y. Wong, J.J. Miles, C.A. Wells, K.J. Radford, Human CD141+ dendritic cell and CD1c+ dendritic cell undergo concordant early genetic programming after activation in humanized mice in vivo, Front. Immunol. 8 (2017) 1419.

[29] T. Lança, J. Ungerbäck, C. Da Silva, T. Joeris, F. Ahmadi, J. Vandamme, M. Svensson-Frej, A.M. Mowat, K. Kotarsky, M. Sigvardsson, W.W. Agace, IRF8 deficiency induces the transcriptional, functional, and epigenetic reprogramming of cDC1 into the cDC2 lineage, Immunity 55 (2022) 1431–1447.e11.

[30] K. Waller, C.L. Scott, Who on IRF are you? IRF8 deficiency redirects cDC1 lineage commitment, Trends Immunol. 43 (2022) 687–689.

[31] V. Durai, P. Bagadia, J.M. Granja, A.T. Satpathy, D.H. Kulkarni, J.T. Davidson, R. Wu, S.J. Patel, A. Iwata, T.T. Liu, X. Huang, C.G. Briseño, G.E. Grajales-Reyes, M. Wöhner, H. Tagoh, B.L. Kee, R.D. Newberry, H.Y. Chang, T.L. Murphy, K.M. Murphy, Cryptic activation of an Irf8 enhancer governs cDC1 fate specification, Nat. Immunol. 20 (9) (2019) 1161–1173.

[32] G.E. Grajales-Reyes, A. Iwata, J. Albring, X. Wu, R. Tussiwand, W. Kc, N.M. Kretzer, C.G. Briseño, V. Durai, P. Bagadia, M. Haldar, J. Schönheit, F. Rosenbauer, T.L. Murphy, K.M. Murphy, Batf3 maintains autoactivation of Irf8 for commitment of a CD8α (+) conventional DC clonogenic progenitor, Nat. Immunol. 16 (7) (2015) 708–717.

[33] T. Hayama, M. Matsuyama, K. Funao, T. Tanaka, K. Tsuchida, Y. Takemoto, Y. Kawahito, H. Sano, T. Nakatani, R. Yoshimura, Beneficial effect of neutrophil elastase inhibitor on renal warm ischemia-reperfusion injury in the rat, Transplant. Proc. 38 (2006) 2201–2202.

[34] Y. Valdez, W. Mah, M.M. Winslow, L. Xu, P. Ling, S.E. Townsend, Major histocompatibility complex class II presentation of cell-associated antigen is mediated by CD8alpha+ dendritic cells in vivo, J. Exp. Med. 195 (2002) 683–694.

[35] C. Hua, L. Sun, Y. Yang, R. Tan, Y. Hou, Mechanisms of CpG-induced CD40 expression on murine bone marrow-derived dendritic cells, Autoimmunity 46 (2013) 177–187.

[36] T.L. Murphy, G.E. Grajales-Reyes, X. Wu, R. Tussiwand, C.G. Briseño, A. Iwata, N.M. Kretzer, V. Durai, K.M. Murphy, Transcriptional control of dendritic cell development, Annu. Rev. Immunol. 34 (2016) 93–119.

[37] B. Cisse, M.L. Caton, M. Lehner, T. Maeda, S. Scheu, R. Locksley, D. Holmberg, C. Zweier, N.S. den Hollander, S.G. Kant, W. Holter, A. Rauch, Y. Zhuang, B. Reizis, Transcription factor E2-2 is an essential and specific regulator of plasmacytoid dendritic cell development, Cell 135 (2008) 37–48.

[38] H.S. Ghosh, B. Cisse, A. Bunin, K.L. Lewis, B. Reizis, Continuous expression of the transcription factor e2-2 maintains the cell fate of mature plasmacytoid dendritic cells, Immunity 33 (2010) 905–916.

[39] B. Deng, Y. Lin, Y. Chen, S. Ma, Q. Cai, W. Wang, B. Li, T. Liu, P. Zhou, R. He, F. Ding, Plasmacytoid dendritic cells promote acute kidney injury by producing interferon-α, Cell. Mol. Immunol. 18 (2021) 219–229.

[40] S.L. Rowland, J.M. Riggs, S. Gilfillan, M. Bugatti, W. Vermi, R. Kolbeck, E.R. Unanue, M.A. Sanjuan, M. Colonna, Early, transient depletion of plasmacytoid dendritic cells ameliorates autoimmunity in a lupus model, J. Exp. Med. 211 (2014) 1977–1991.

[41] S. Carotta, S.N. Willis, J. Hasbold, M. Inouye, S.H. Pang, D. Emslie, A. Light, M. Chopin, W. Shi, H. Wang, H.C. Morse, D.M. Tarlinton, L.M. Corcoran, P. D. Hodgkin, S.L. Nutt, The transcription factors IRF8 and PU.1 negatively regulate plasma cell differentiation, J. Exp. Med. 211 (2014) 2169–2181.

[42] R.M. Kratofil, P. Kubes, J.F. Deniset, Monocyte conversion during inflammation and injury, Arterioscler. Thromb. Vasc. Biol. 37 (2017) 35–42.

[43] D. Kurotaki, N. Osato, A. Nishiyama, M. Yamamoto, T. Ban, H. Sato, J. Nakabayashi, M. Umehara, N. Miyake, M. Matsumoto, M. Nakazawa, K. Ozato, T. Tamura, Essential role of the IRF8-KLF4 transcription factor cascade in murine monocyte differentiation, Blood 121 (2013) 1839–1849.

[44] A. Yáñez, S.G. Coetzee, A. Olsson, D.E. Muench, B.P. Berman, D.J. Hazelett, N. Salomonis, H.L. Grimes, H.S. Goodridge, Granulocyte-monocyte progenitors and monocyte-dendritic cell progenitors independently produce functionally distinct monocytes, Immunity 47 (2017) 890–902.e4.

[45] Y. Komano, T. Nanki, K. Hayashida, K. Taniguchi, N. Miyasaka, Identification of a human peripheral blood monocyte subset that differentiates into osteoclasts, Arthritis Res. Ther. 8 (2006) R152.

[46] J. Hettinger, D.M. Richards, J. Hansson, M.M. Barra, A.C. Joschko, J. Krijgsveld, M. Feuerer, Origin of monocytes and macrophages in a committed progenitor, Nat. Immunol. 14 (2013) 821–830.

[47] K.S. Shin, K. Jeon, B.S. Kim, I.K. Kim, Y.J. Park, C.H. Koh, B. Song, J.M. Lee, J. Lim, E.A. Bae, H. Seo, Y.H. Ban, S.J. Ha, C.Y. Kang, Monocyte-derived dendritic cells dictate the memory differentiation of CD8+ T cells during acute infection, Front. Immunol. 10 (2019) 1887.

[48] C. Bosteels, K. Neyt, M. Vanheerswynghels, M.J. van Helden, D. Sichien, N. Debeuf, S. De Prijck, V. Bosteels, N. Vandamme, L. Martens, Y. Saeys, E. Louagie, M. Lesage, D.L. Williams, S.C. Tang, J.U. Mayer, F. Ronchese, C.L. Scott, H. Hammad, M. Guilliams, B.N. Lambrecht, Inflammatory type 2 cDCs acquire features of cDC1s and macrophages to orchestrate immunity to respiratory virus infection, Immunity 52 (2020) 1039–1056.e9.

[49] K. Sasaki, A.S. Terker, Y. Pan, Z. Li, S. Cao, Y. Wang, A. Niu, S. Wang, X. Fan, M.Z. Zhang, R.C. Harris, Deletion of myeloid interferon regulatory factor 4 (Irf4) in mouse model protects against kidney fibrosis after ischemic injury by decreased macrophage recruitment and activation, JASN (J. Am. Soc. Nephrol.) 32 (2021) 1037–1052.

[50] M. Lech, C. Römmele, R. Gröbmayr, H. Eka Susanti, O.P. Kulkarni, S. Wang, H.J. Gröne, B. Uhl, C. Reichel, F. Krombach, C. Garlanda, A. Mantovani, H. J. Anders, Endogenous and exogenous pentraxin-3 limits postischemic acute and chronic kidney injury, Kidney Int. 83 (2013) 647–661.

[51] D. Nakazawa, S.V. Kumar, J. Marschner, J. Desai, A. Holderied, L. Rath, F. Kraft, Y. Lei, Y. Fukasawa, G.W. Moeckel, M.L. Angelotti, H. Liapis, H.J. Anders, Histones and neutrophil extracellular traps enhance tubular necrosis and remote organ injury in ischemic AKI, JASN (J. Am. Soc. Nephrol.) 28 (2017) 1753–1768.

[52] T. Hayama, M. Matsuyama, K. Funao, T. Tanaka, K. Tsuchida, Y. Takemoto, Y. Kawahito, H. Sano, T. Nakatani, R. Yoshimura, Beneficial effect of neutrophil elastase inhibitor on renal warm ischemia-reperfusion injury in the rat, Transplant. Proc. 38 (2006) 2201–2202.

[53] J. Lee, Y.J. Zhou, W. Ma, W. Zhang, A. Aljoufi, T. Luh, K. Lucero, D. Liang, M. Thomsen, G. Bhagat, Y. Shen, K. Liu, Lineage specification of human dendritic cells is marked by IRF8 expression in hematopoietic stem cells and multipotent progenitors, Nat. Immunol. 18 (2017) 877–888.

[54] T. Tamura, D. Kurotaki, S. Koizumi, Regulation of myelopoiesis by the transcription factor IRF8, Int. J. Hematol. 101 (2015) 342–351.